IEEE Access
Multidisciplinary | Rapid Review | Open Access Journal

Received October 23, 2019, accepted November 7, 2019, date of publication November 13, 2019, date of current version December 5, 2019.

Digital Object Identifier 10.1109/ACCESS.2019.2953302

Development and Hybrid Control of an Electrically Actuated Lower Limb Exoskeleton for Motion Assistance

CHAO-FENG CHEN[1], ZHI-JIANG DU[1], (Member, IEEE), LONG HE[2], YONG-JUN SHI[1], JIA-QI WANG[1], GUO-QIANG XU[2], YU ZHANG[2], DONG-MEI WU[1], AND WEI DONG[1], (Senior Member, IEEE)

[1]State Key Laboratory of Robotics and System, Harbin Institute of Technology (HIT), Harbin 150001, China
[2]China South Industries Group Corporation, Weapon Equipment Research Institute, Beijing 102202, China

Corresponding author: Wei Dong (dongwei@hit.edu.cn)

This work was supported by the pre-research project in the manned space field of China under Project 020202.

ABSTRACT This paper describes a system design and hybrid control algorithm of an electrically actuated lower limb exoskeleton (LLE). The system design mainly includes three parts: mechanical structure design, actuation system design and sensor system design. According to the initial state of the joint angle, LLE can be divided into Non-anthropomorphic state (NAS) and anthropomorphic state (AS). The human motion intention (HMI) estimation can be divided into gait phase classification and reference trajectory estimation. The fuzzy logic is used to detect different phases in the gait phase classification. In the reference trajectory estimation, the kinematic model of the LLE is utilized to obtain a continuous joint trajectory, which is used as input of the control law. To make the LLE accurately follow the movement of people and remain stable, a hybrid dual-mode control strategy is proposed in this paper, i.e., the adaptive impedance control (AIC) method is used to improve the stability and resistance to shock in stance phase, and the active disturbance rejection control with the fast terminal sliding mode control (ADRC-FTSMC) method is employed to improve the response speed and the tracking precision in swing phase. Furthermore, in order to solve the torque discontinuity in the switching process, a smoothing method is proposed during the transition. Finally, the prototype experiments were set up to verify the tracking performance and power-assisted effect of the proposed exoskeleton. The experiments results show the LLE can achieve excellent tracking performance and power-assisted effect based on the proposed HMI methodology and hybrid dual-mode control strategy.

INDEX TERMS Lower limb exoskeleton, system design, human motion intention, hybrid dual-mode control, tracking performance, power-assisted effect.

I. INTRODUCTION

Recently, the development of lower limb exoskeletons (LLEs) that improve the strength and endurance of human users has received widespread attention [1]–[3]. The LLEs are expected to provide additional power for human motion, which can be used in various fields such as military, industrial and medical rehabilitation. Many advanced exoskeletons have been made in the past two decades. For instance, in 2004, the research team at the UC Berkeley developed the Berkeley Lower Extremity Exoskeleton (BLEEX) to enhance users walking ability and assist users in carrying heavy loads [4], [5]. Based on the BLEEX system, ExoHiker, ExoClimber and HULC are developed in later years, which simplify the mechanical structure and remove the active hip drive [6]. Furthermore, Raytheon-Sarcos developed the XOS2 in 2010 [7], [8], which is a relatively complete full-body exoskeleton to date (i.e., includes arms and legs). According to the reports, the user wears the XOS2 can manipulate 100 pounds payloads and the self-weight of the system can reach 95kg. From 2002 to 2010, the research group at the University of Tsukuba developed the hybrid assistive limb (HAL) to improve the life quality of patients with hemiplegia, which sends the command signal applying the bioelectrical signal [9]–[11]. Moreover, RB3D Company developed the HERCULE for the French Ministry of Defense in 2012, which arranges two sets of

The associate editor coordinating the review of this manuscript and approving it for publication was Yanzheng Zhu.

FIGURE 1. The prototype of HEXO system.

electrical servo actuators on the knee and hip joints [12]. Besides those, Argo Medical Technologies of Israel unveiled the ReWalk series for independent walking of patients with spinal cord injury, which also made significant contributions to the research of LLEs [13]. Despite those efforts, there are still many challenges in the architecture design, the human motion intention estimation and the control strategy design.

The architecture design is a significant aspect of the development of the LLEs, which can be divided into anthropomorphic design and non-anthropomorphic design [14]. Notice that most of the mechanical architectures use anthropomorphic design to make LLEs' structure be aligned with the wearer lower limbs. However, there is a dead point on the anthropomorphic structure when the LLE stands in a straight state. To avoid the dead point of the knee joint at 0 degree, a non-anthropomorphic LLE is proposed. This design makes the LLE in a ''squat state'' when the wearer is in a straight state. Besides, the actuation system is also an indispensable part of the LLEs. The currently popular actuation systems are hydraulic actuators and electrical actuators, which have a high torque-mass rates [15]. Considering the heavy weight and difficult maintenance of the hydraulic actuator, the LLE choose the electrical actuator to parallel with the joint of the mechanical leg, which makes the joint structure compact and easy to control. In this paper, an electrically actuated non-anthropomorphic LLE called HEXO (a Harbin Institute of Technology's exoskeleton) was developed, as shown in Figure 1.

The most ideal LLE is to allow users to move comfortably according to their human motion intention (HMI) and feel less interaction force. The HMI can be obtained by large quantities of interaction information between human and LLE, which is a critical part in the LLE control loop [16]. The interaction information can be divided into two kinds of classification, i.e., biomedical information and physical information. The typical biomedical information includes the surface electromyography (sEMG) signals and electroencephalograph (EEG) signals. The sEMG signal is widely used in rehabilitation [17]. The rehabilitation devices can incorporate the information extracted from sEMG and recognize the motion patterns [18]. Through the brain-machine interface, the EEG signals can be used to operate the exoskeleton in real-time [19]. However, the function of the biomedical signals will be affected by the individual difference. The physical information contains the force and torque signals. Those signals are commonly generated by sensors embedded in bundle connectors, which are located at the connection with the trunk, thigh, calf and foot [20], [21]. To acquire the accurate interaction information, the connection bundle will be tied tightly. Therefore, the designed HEXO system binds the foot and trunk to detect interaction forces. Besides, the HMI estimation is divided into two procedures, i.e., the gait phase classification and the reference trajectory estimation. In the gait phase classification, the fuzzy logic is used to divide the human gait phase into four sub-phases, i.e., Initial Contact (IC), Mid Stance (MSt), Initial Swing (ISw), and Swing (Sw). In the reference trajectory estimation, the kinematic model is employed to calculate the desired joint trajectory of the HEXO.

The core of an LLE system is the control strategy, which determines the performance of the system. There are many control strategies in previous studies [22]. It mainly includes sensitivity amplification control (SAC) [23], predefine gait trajectory control (PGTC) [24], and model-based control (MBC) [25]. However, SAC is too sensitive to external disturbances, PGTC has poor adaptability to randomness movement, and MBC requires accurate dynamic model. Therefore, more and more LLEs choose the hybrid assistive control to solve the problems [26]. Since its excellent performance, hybrid assistive control becomes a more popular control strategy. During a gait cycle, the active joint moves fast in the swing phase, although it needs to support the weight of an LLE and resist the impact in the support phase. Based on those characteristics, a hybrid dual-mode control based on HMI is proposed. That is, in the swing phase, the HEXO uses the active disturbance rejection control with the fast terminal sliding mode control (ADRC-FTSMC) to track the desired trajectory fast, which is called the AF mode. In addition, in the stance phase, the HEXO uses the adaptive impedance control (AIC) to support the system stable, which is called the AI mode.

In summary, the main contributions of this paper can be summarized as follows.

1) A novel LLE called HEXO is developed, including its mechanical structure, actuation system and sensor system.

2) A hybrid HMI estimator is proposed, which can be divided into gait phase classification and reference trajectory estimation.

3) A hybrid dual-mode control based on HMI is proposed.

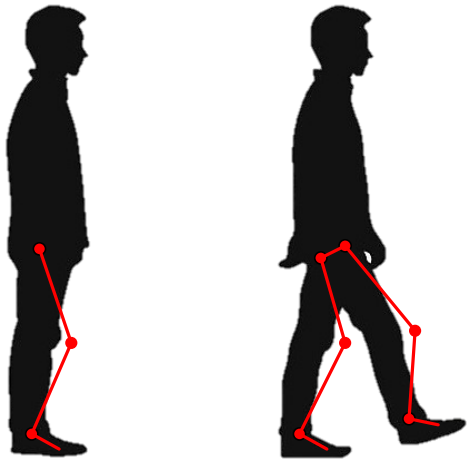

FIGURE 2. A non-anthropomorphic LLE structure sketch.

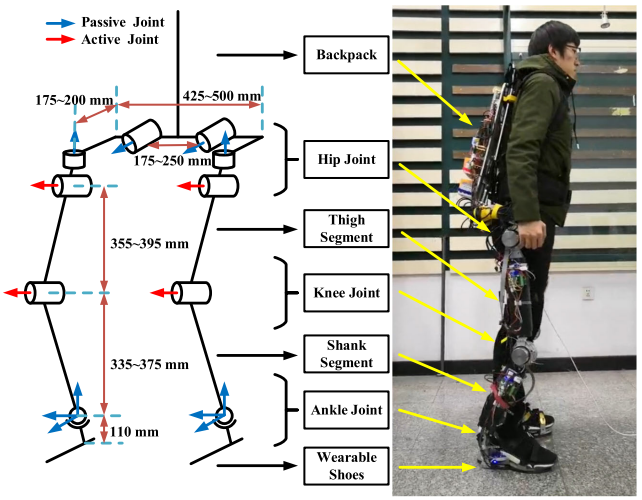

FIGURE 3. The mechanical structure of HEXO.

4) The performance of HEXO was evaluated by experiments, including squatting, walking, and going up/down stairs.

The rest of the paper is organized as follows. In Section II, the design and sensor system of the HEXO is presented. A hybrid HMI estimator including gait phase classification and reference trajectory estimation is designed in Section III. A hybrid dual-mode control is shown in Section IV, which illustrates the ADRC-FTSMC and AIC control method. Experiments of the HEXO using the proposed HMI estimator and dual-mode control are conducted in Section V. Finally, the conclusion and future work is drawn in Section VI.

II. SYSTEM DESIGN FOR HEXO

Since the LLE is a wearable device, its degrees of freedom (DOFs) should be similar to those of the human lower limb. However, if the LLE is a straight configuration in the initial state, it will cause singularities in the knee joint. Therefore, the HEXO is designed as a non-anthropomorphic LLE to eliminate singularities, whose knee joint is not corresponding to the user (Fig. 2). In this section, the electrically actuated non-anthropomorphic HEXO is described, which includes the mechanical structure, actuation system, and sensor system.

A. MECHANICAL STRUCTURE DESIGN

The mechanical structure of HEXO is shown in Fig. 3. The HEXO consists of backpack, hip joint, thigh segment, knee joint, shank segment, ankle joint and wearable shoes. The power unit, the control system and the data collection system are installed into the backpack. Each leg of the HEXO possesses seven DOFs, i.e., hip flexion/extension (HFE), hip adduction/abduction (HAA), hip internal/external (HIE), knee flexion/extension (KFE), ankle plantar flexion / dorsiflexion (APD), ankle eversion/inversion (AEI), and ankle internal/external (AIE). Since the movement of the HEXO is mainly facilitated in the sagittal plane, the hip flexion/extension and knee flexion/extension are actuated, while the other DOFs are passive. To reduce the complexity of the HEXO, the actuated joints are driven by the DC motors directly, i.e. the motors' shafts are corresponded to rotation axes of the actuated joints. In addition, to develop a lightweight HEXO, the carbon fiber is selected to make of the thigh segment and the shank segment. The HEXO weighs 25 kg and can reach the speed up to 4 km/h.

TABLE 1. Joint range of motion of HEXO.

Joint	Axis	Type	HEXO range	Normal range	Human Max range
Hip	HFE	Active	-30°~120°	-13°~105°	-35°~130°
	HAA	Passive	-20°~30°	-16°~20°	-30°~50°
	HIE	Passive	-20°~30°	-15°~18°	-30°~45°
Knee	KFE	Active	-120°~0°	-110°~0°	-150°~0°
Ankle	APD	Passive	-30°~30°	-28°~25°	-40°~35°
	AEI	Passive	-20°~20°	-16°~15°	-25°~20°
	AIE	Passive	-20°~20°	-18°~14°	-30°~20°

The length of thigh and shank segments can be adjusted through the adjustment mechanisms, which makes the HEXO leg matches the human leg. One end of the adjustment mechanism is fixed to the joint, and the other end is connected to the segment via screw bolts. According to the body dimensions and body proportions of users [27], the designed adjustment ranges of each segment are given in Fig. 3. Such design can fit users of different heights (165-185cm). To ensure normal movement of the user without restriction, the range of motion for each joint of HEXO was designed to be larger than that of normal movement. Meanwhile, to ensure the user's safety, the range of motion of each joint was designed to be smaller than the maximum range of human motion. The range of motion of each joint is shown in Table 1.

The backpack and the wearable shoes are the key parts of the human machine interaction, which are designed in a hierarchical structure. The backpack includes the inner layer and outer layer, as shown in Fig. 4. The inner layer is used to tie the shoulder and waist of the user via flexible strap. The outer layer is used to place the power supply, control

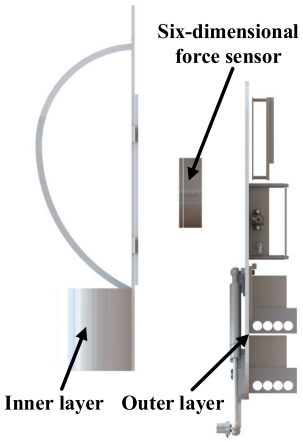

FIGURE 4. The backpack includes the inner layer and outer layer.

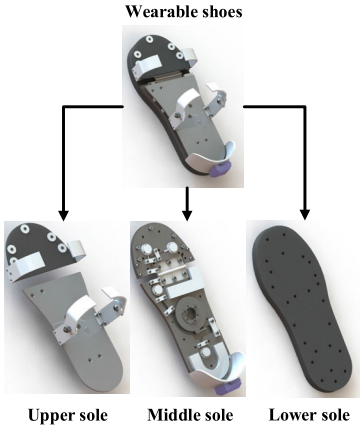

FIGURE 5. The wearable shoes include the upper sole, middle sole and lower sole.

board, and data collection card. The six-dimensional sensor is placed between the inner layer and outer layer for connection, which can accurately measure the motion intention of human back. The wearable shoes can be divided into upper sole, middle sole and lower sole, as shown in Fig.5. The upper sole is employed to fasten the foot of the user via buckles. The middle sole is used to place the pressure sensors and the six-dimensional force sensor. The lower sole is made of rubber pad, which can alleviate the impact of foot landing. To fit the user foot bending comfortably, both the middle sole and the upper sole are designed as two parts. In middle sole, the front part and the back part are connected by a hinge. In upper sole, the front part and the back part are not directly connected while these two parts are connected indirectly through the middle sole. The front part of upper sole and the middle sole are connected by screw bolt. The back part of upper sole and the middle sole are connected by six-dimensional force sensor, which can measure the human intention via foot movement. Besides, the ''L'' and ''U'' shape rubber are inserted into the middle sole to protect the sensors.

B. ACTUATION SYSTEM DESIGN

The main function of the actuation system is to transfer the drive command generated by the control system to the HEXO

TABLE 2. The specification of actuation system.

Joint	Axis	Peak torque	Nominal torque	Peak speed	Nominal speed
Hip	HFE	67Nm	28.9Nm	60rpm	37.4rpm
Knee	KFE	54Nm	23.1Nm	75rpm	46.8rpm

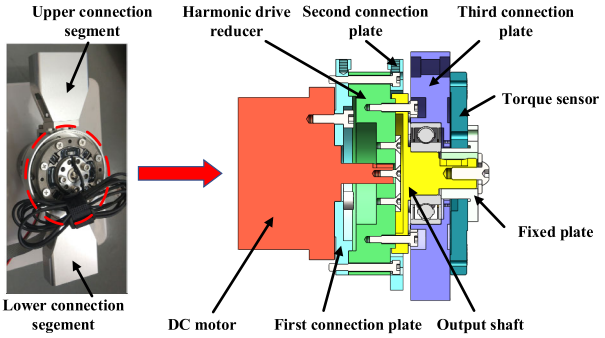

FIGURE 6. The joint construction of the HEXO.

movement. The actuation system is powered by a brushless DC motor (type: EC 60 flat, Maxon Motor, Switzerland), which is efficient and reliable. The incremental encoder (type: MILE Encoder 1024 CPT, Maxon Motor, Switzerland) is integrated into the motor. To guarantee the joint torque, the motor in HFE is combined with a harmonic drive with ratio 1:100 (type: LHD 17-100, LEADERDRIVE, China), and the motor in KFE is combined with a harmonic drive reducer with ratio 1:80 (type: LHD 17-80, LEADERDRIVE, China). The servo drivers of these motors are arranged on the thigh segment and the shank segment respectively (type: G-SOLTWI 10/100SE, ELMO, Israel). The specification of these combinations is listed in Table 2.

The hip joint construction is the same as the knee joint, as shown in Fig. 6. It consists of DC motor, harmonic drive, output shaft, torque sensor, fixed plate and three connection plates. The shaft of the DC motor is connected to the wave generator of the harmonic drive reducer via a flat key. The rigid gear of the harmonic drive reducer is connected to the output shaft through screw bolts. The end of the output shaft is connected to the fixed plate via a flat key. The fixed plate is connected to the inner ring of the torque sensor through screw bolts. The outer ring of the torque sensor is connected to the third connection plate via screw bolts. The first connection plate and the second connection plate are used to connect the upper connection segment. The third connection plate is used to connect the lower connection segment. In the hip joint, the upper connection plate is connected to the waist structure of HEXO and the lower connection is connected to the thigh segment. In the knee joint, the upper connection plate is connected to the thigh segment and the lower connection is connected to the shank segment. Each powered joint has a weight of 1.79 kg and a power of 200 W, which can run for 4 hours.

To develop a non-anthropomorphic LLE, the joint of HEXO is designed to have a certain angle in initial state,

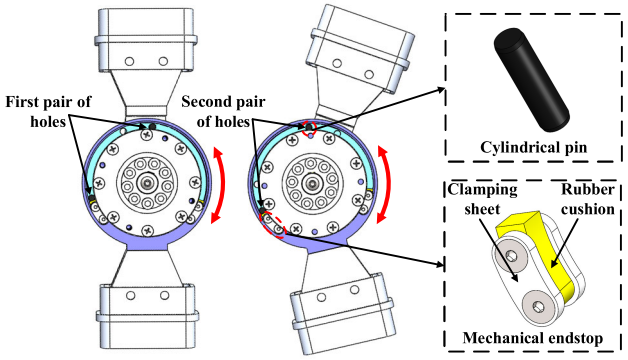

FIGURE 7. Anthropomorphic joint and non-anthropomorphic joint.

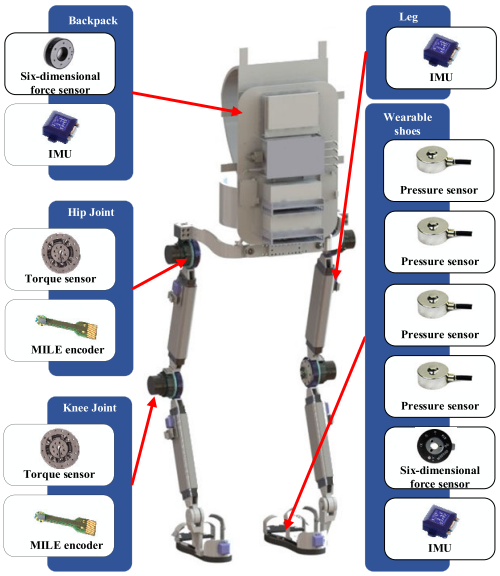

FIGURE 8. Sensor configuration.

as shown in Fig. 7. The mechanical limiting device, which consists of a mechanical end-stop and a cylindrical pin, is designed to achieve the non-anthropomorphic knee joint. This design method is relatively straightforward and easy to implement. The mechanical end-stop integrated in the third connection plate uses two clamping sheets to clamp the rubber cushion, which can absorb shock and improve the spring stabilization of the joint. To compare the performance of the non-anthropomorphic LLE and the anthropomorphic LLE, two pairs of limiting holes are designed on the second connection plate. The first pair of holes is used to keep the HEXO straight in initial state. The second pair of holes is used to keep the HEXO with a certain angle in initial state, which make the thigh segment and shank segment at an angel of 30°.

C. SENSOR SYSTEM DESIGN

The sensor configuration of the HEXO is shown in Fig. 8. The six-dimensional force sensor (SFS) (type: M3715D, SRI, China) and inertial measurement unit (IMU) (type:

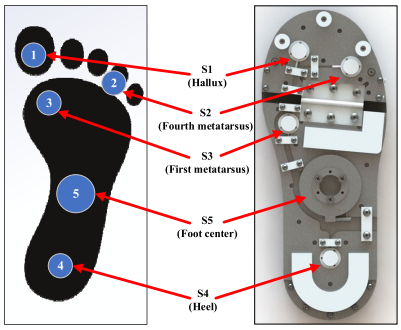

FIGURE 9. Foot sensor arrangement.

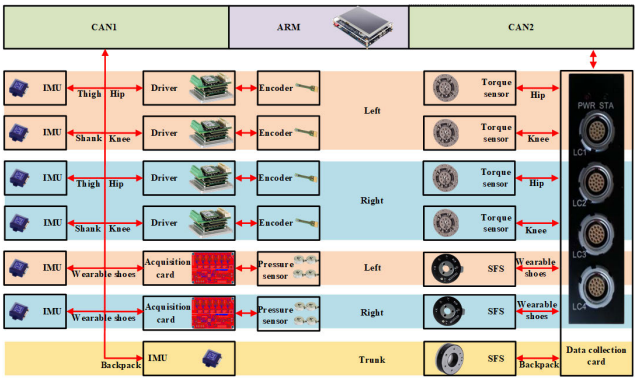

FIGURE 10. Sensor system network.

LPMS-CU2, ALUBI, China) are placed at the backpack, which are used to measure the human machine interaction and angle of the trunk. The torque sensor (type: 2210C, SRI, China) and the incremental encoder are placed at hip and knee joint, which are used to measure the torque and angle of the joint. To avoid the signal burrs caused by the angular difference, the IMU placed at the thigh segment and the shank segment are used to acquire the angular velocity and angular acceleration of the joint.

Four pressure sensors (type: AT8106, AUTODA, China), an SFS (type: M3554E, SRI, China) and an IMU are placed at the wearable shoes, which are used to measure the plantar interaction force and the ankle angle. Given that the plantar interaction distribution of human movement, the arrangement of four pressure sensors and an SFS are shown in Fig. 9. The four pressure sensors are located respectively in hallux, fourth metatarsus, first metatarsus and heel. The SFS is located in the center of the foot.

Fig. 10 shows the sensor system network of the HEXO. All sensor data is transmitted to ARM (type: ARM-Cortex-A9, ARM, UK) through CAN (Controller Area Network) bus, whose transmission rate is up to 1Mbits. The ARM has dual CAN ports. All joint encoders, plantar pressure sensors and IMUs communicate with ARM via CAN1 port. The Elmo driver collects the data of the encoder and transmits it to the ARM. The acquisition card is used to convert the collected pressure sensor analog signals into digital signals

and transmit them to the ARM. All joint torque sensors and SFSs communicate with ARM via CAN2 port. The data collection card (type: M8127, SRI, China) has four channels to collect the sensor data. Channel LC1 responds to the four torque sensors. Channel LC2 responds to the SFS on the left wearable shoes. Channel LC3 responds to the SFS on the right wearable shoes. Channel LC4 responds to the SFS on the backpack.

III. METHOD FOR HMI ESTIMATION

The HMI generated by the brain is converted into human body movement. This movement causes the limbs to contact with the exoskeleton to generate interaction forces. Therefore, the estimation of HMI can be reflected by the interaction forces. In this section, the HMI estimation is divided into two procedures, i.e., gait phase classification and reference trajectory estimation. Firstly, the gait phase classification uses the fuzzy logic to detect IC, MSt, ISw and Sw. Second, the reference trajectory estimation uses the kinematic model of HEXO to obtain a continuous joint trajectory that is used as input of the control method. Those two procedures can be combined to satisfy the need of HMI estimation in lower limb. The details of two procedures are discussed as below.

A. GAIT PHASE CLASSIFICATION

The gait phase of human body is judged by the plantar interaction forces based on the pressure distribution of the sole [28]. During the walking process, most of the body weight is exerted on hallux, first metatarsus, fourth metatarsus and heel. Therefore, the four pressure sensors collect the pressure values of these four positions, which are termed as FS1, FS2, FS3 and FS4. Since the weight and walking way are different for different wearers, the magnitude of the pressure is a vague concept. Therefore, the pressure value should be normalized, as shown below,

$$P_{si} = \frac{F_{si}}{F_{s1} + F_{s2} + F_{s3} + F_{s4}} \tag{1}$$

where P_{Si} is the normalized data at S_i. To distinguish 'large' and 'small' pressure, sigmoid function is used as the membership function [29], which is defined as follows,

$$f_{large}\,(P_{Si}) = \frac{1}{1 + e^{-P_{Ai}(P_{Si} - P_{Ci})}} \tag{2}$$

$$f_{small}\,(P_{Si}) = 1 - f_{large}\,(P_{Si}) \tag{3}$$

where P_{Ai} is a sensitivity coefficient, P_{Ci} is a proportional coefficient, and e is exponential function. It observes that when the '$f_{large}(P_{Si})$' value is larger than P_{Ci}, the pressure is 'Large' and when the '$f_{small}(P_{Si})$' value is larger than P_{Ci}, the pressure is 'Small', respectively.

According to the gait phase divided by the human walking gait theory, the design fuzzy rules are list in Table 3. The IC phase is detected when 'Large' force is exerted on S1, while the remaining position measure 'Small' forces. The MSt phase is detected when 'Large' force is generated at four locations. The ISw phase is detected when 'Small' force is exerted on S4, while the remaining position measure 'Large'. The Sw phase is detected when 'Small' force is generated at four locations.

TABLE 3. Fuzzy rules for gait phase classification.

S1	S2	S3	S4	State	Gait Phase
Small	Small	Small	Large		IC
Large	Large	Large	Large		MSt
Large	Large	Large	Small		ISw
Small	Small	Small	Small		Sw

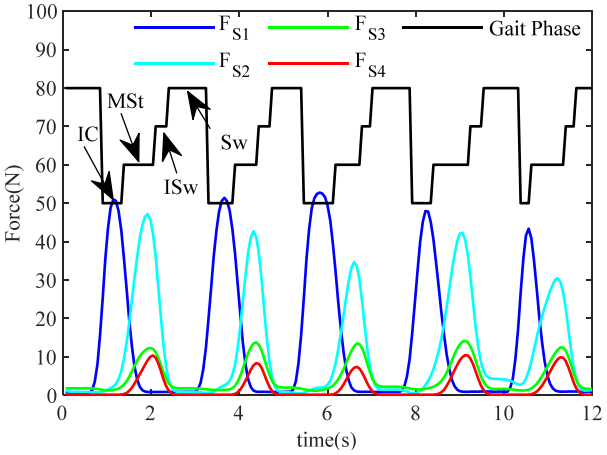

FIGURE 11. Plantar pressure signals obtained from the four pressure sensors and the four gait phases detected during walking.

To make the gait phase classification match the characteristics of human walking, the coefficient of the membership function are set as $P_{A1} = 10$, $P_{A2} = 2$, $P_{A3} = P_{A4} = 1$, $P_{C1} = 0.1$, and $P_{C2} = P_{C3} = P_{C4} = 0.05$. According to Table 3 and the membership functions, the gait phase classificationn result is shown in Fig. 11.

B. REFERENCE TRAJECTORY ESTIMATION

Reference trajectory estimation can be used as input commands to control the HEXO. The desired trajectory of the HEXO is used to match the wearer's movement trajectory. It is difficult to directly measure the joint movement of the human body, because it needs to fit complex sensors on the wearer, which is hard to fix and makes the wearer uncomfortable. Therefore, a trajectory estimation method for estimating human motion trajectory using human-machine interaction force is proposed. The interaction force is detected by the SFS, which is mounted on the backpack and the foot between the wearer and the HEXO. In order to obtain the relationship between interaction force and desired trajectory, the kinematic models of sagittal plane are established, as shows in Fig. 12. This allows the four gait phases above to be divided into a stance phase and a swing phase. The kinematic model of HEXO can be simplified to a three-link mechanism in the stance phase and a two-link mechanism in

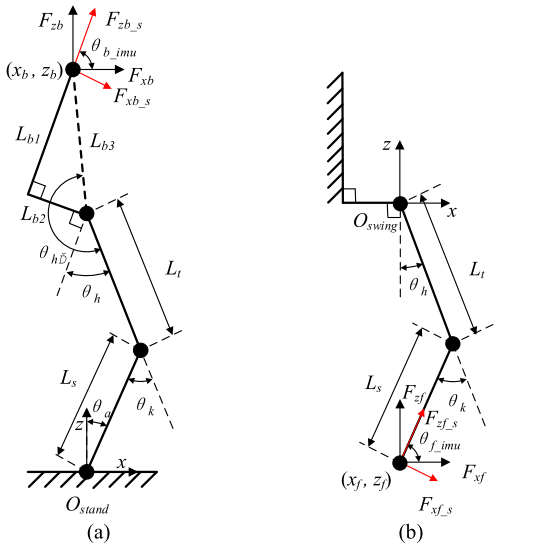

FIGURE 12. The kinematic model. (a) stance phase, (b) swing phase.

the swing phase. In stance phase, the foot is considered as a fixed base and the backpack is considered as a free end. In the swing phase, the backpack is regarded as a fixed base and the foot is considered as a free end. The free end acts as the kinematic terminal. The positional function of the terminal points in the corresponding base coordinate system can be obtained as follows,

$$\begin{bmatrix} x_b \\ z_b \end{bmatrix} = \begin{bmatrix} L_s \sin\theta_a - L_t \sin(\theta_k - \theta_a) - L_{b3} \sin(\theta_{h'} - \theta_k + \theta_a) \\ L_s \cos\theta_a + L_t \cos(\theta_k - \theta_a) - L_{b3} \cos(\theta_{h'} - \theta_k + \theta_a) \end{bmatrix} \tag{4}$$

$$\begin{bmatrix} x_f \\ z_f \end{bmatrix} = \begin{bmatrix} L_t \sin\theta_h - L_s \sin(\theta_k - \theta_h) \\ -L_t \cos\theta_h - L_s \cos(\theta_k - \theta_h) \end{bmatrix} \tag{5}$$

where L_s is the length of shank and L_t is the length of thigh; $L_{b3} = (L_{b1} + L_{b2})^{1/2}$ is the length of virtual link in the stance phase; L_{b1} and L_{b2} are the length and width of backpack; θ_h, θ_k and θ_a are angle of hip, knee and ankle; $\theta_{h'} = \theta_h + \pi/2 +$ atan(L_{b1}/L_{b2}) is the virtual hip angle in the stance phase.

The human-machine interaction forces measured by the SFSs are converted to the corresponding coordinate system through coordinate transformation. After transformation, the terminal forces can be expressed as follows,

$$\begin{bmatrix} F_{xb} \\ F_{zb} \end{bmatrix} = \begin{bmatrix} F_{xb\_s} \sin(\theta_{b\_imu}) + F_{zb\_s} \cos(\theta_{b\_imu}) \\ F_{zb\_s} \sin(\theta_{b\_imu}) - F_{xb\_s} \cos(\theta_{b\_imu}) \end{bmatrix} \tag{6}$$

$$\begin{bmatrix} F_{xf} \\ F_{zf} \end{bmatrix} = \begin{bmatrix} F_{xf\_s} \sin(\theta_{f\_imu}) + F_{zf\_s} \cos(\theta_{f\_imu}) \\ F_{zf\_s} \sin(\theta_{f\_imu}) - F_{xf\_s} \cos(\theta_{f\_imu}) \end{bmatrix} \tag{7}$$

where θ_{b_imu} and θ_{f_imu} are measured by the IMU to represent the angle of the backpack and shoes. Therefore, the terminal trajectory can be estimated as [30],

$$\begin{bmatrix} x_b(k) \\ z_b(k) \end{bmatrix} = \begin{bmatrix} x_b(k-1) + F_{xb}/K_{xb} \\ z_b(k-1) + F_{zb}/K_{zb} \end{bmatrix} \tag{8}$$

$$\begin{bmatrix} x_f(k) \\ z_f(k) \end{bmatrix} = \begin{bmatrix} x_f(k-1) + F_{xf}/K_{xf} \\ z_f(k-1) + F_{zf}/K_{zf} \end{bmatrix} \tag{9}$$

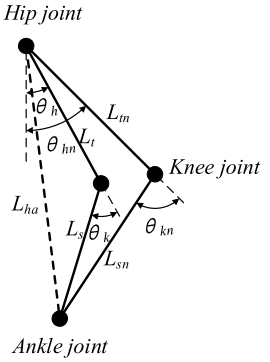

FIGURE 13. The structure sketch in the two states.

where K_{xb}, K_{zb}, K_{xf} and K_{zf} denote the human's stiffness; $(x_b(k\text{-}1), z_b(k\text{-}1))$ and $(x_f(k\text{-}1), z_f(k\text{-}1))$ can be obtained by fomula (4) and fomula (5). The desired velocity of the terminal point can be obtained by the desired trajectory. According to the inverse kinematics principle, the desired joint angular velocity of each joint can be calculated as follows,

$$\begin{bmatrix} \dot{q}_h(k) \\ \dot{q}_k(k) \end{bmatrix} = J^{-1} v(k) = J^{-1} \begin{bmatrix} \dot{x}(k) \\ \dot{z}(k) \end{bmatrix} \tag{10}$$

where J is the velocity Jacobian matrix and $v(k)$ is the velocity of the terminal point.

Through the process above, the reference trajectory of each joint can be obtained. This trajectory is applied to the HEXO in the anthropomorphic state, and the trajectory in the non-anthropomorphic state needs to be converted. In the non-anthropomorphic state, the hip and ankle rotation axes of the HEXO are aligned with the corresponding joints of the human body, while the HEXO knee rotation axis is not aligned with the human knee joint. In the anthropomorphic state, the axes of the three joints are aligned to the human joint. Based on this, the structure sketch in the two states is shown as Fig. 13.

The length from the hip to the ankle is fixed, which can be obtained as follows.

$$L_{ha} = \sqrt{L_t^2 + L_s^2 - 2L_t L_s \cos(\pi - \theta_k)} \tag{11}$$

Furthermore, the angle of the knee joint in the non-anthropomorphic state can be expressed as follows,

$$\theta_{kn} = \pi - \arccos \frac{L_{tn}^2 + L_{sn}^2 - L_{ha}^2}{2L_{tn}L_{sn}} \tag{12}$$

where L_{tn} and L_{sn} are the length of thigh and shank in the non-anthropomorphic state. The angle of hip joint in the non-anthropomorphic state can be expressed as follows.

$$\theta_{hn} = \theta_h + \left(\arccos \frac{L_{tn}^2 + L_{ha}^2 - L_{sn}^2}{2L_{tn}L_{ha}} - \arccos \frac{L_t^2 + L_{ha}^2 - L_s^2}{2L_t L_{ha}} \right) \tag{13}$$

Finally, the actual reference trajectory of each joint is obtained as follows,

$$\begin{bmatrix} \theta_{kn\_r} \\ \theta_{hn\_r} \end{bmatrix} = \begin{bmatrix} \theta_{kn} - \theta_{kn\_0} \\ \theta_{hn} - \theta_{hn\_0} \end{bmatrix} \tag{14}$$

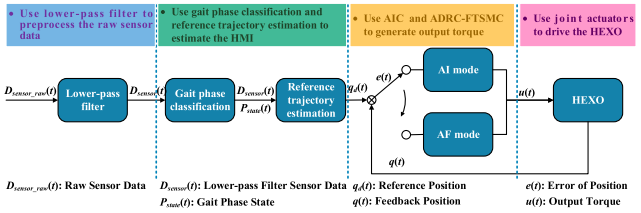

FIGURE 14. The control flow of HEXO.

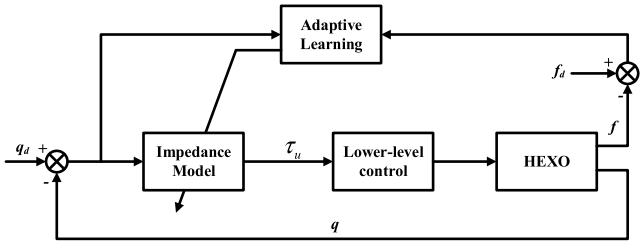

FIGURE 15. The AIC control architecture.

where θ_{kn_r} and θ_{hn_r} are the actual rotation angles of the knee and the hip joints; θ_{kn_0} and θ_{hn_0} are the initial angles of the knee and the hip joints.

IV. METHOD FOR HMI ESTIMATION

The goal of the hybrid control is to make HEXO accurately follow the movement of the person and keep stable. The control flow of HEXO is shown in Fig. 14. First, the raw sensor data is processed by a low-pass filter. Second the HMI is estimated by the gait phase classification and the reference trajectory. Third, the output torques are generated by the hybrid dual-mode control. Finally, the HEXO is driven by joint actuators. In stance phase, the joint has a smaller angle of motion but a heavier load, which requires high stability and strong shock resistance. In swing phase, the joint has a smller load but a larger angle of motion, which means fast response and precise tracking. Therefore, the AIC method is used to improve the stability and shock resistance in stance phase, and the ADRC-FTSMC method is adopted to improve the response speed and the tracking precision in swing phase. Besides, to achieve smooth switching from AI mode to AF mode or from AF mode to AI mode, a smoothing method is proposed during the transition in IC phase and ISw phase.

A. DUAL-MODE CONTROL METHOD

Considering the motion characteristics of the stance phase and the swing phase, a dual-mode control method is proposed. In AI mode, the AIC method is proposed to improve joint impact resistance while following human movement. In AF mode, the ADRC-FTSMC method is proposed to improve tracking accuracy and response speed. The specific implementation of ADRC-FTSMC method has been detailedly introduced in previous work [31]. A detailed explanation of AIC method will be discussed as below.

The objective of AI mode is to control the interaction between the HEXO and the user, so an AIC control architecture is proposed as shown in Fig. 15. The dynamics of the HEXO in the joint space are given by,

$$M(q)\ddot{q} + C(q,\dot{q})\dot{q} + G(q) = \tau_u + \tau_h \tag{15}$$

where $M(q)$ is the inertia matrix, $C(q)$ is the Coriols matrix and $G(q)$ is the gravity term, respectively, τ_u is the control torque, and τ_h denotes the interaction torque exerted by the user. The target impedance model can be expressed as follows,

$$\begin{aligned} M_d(t)\left(\ddot{q}_d(t) - \ddot{q}(t)\right) + B_d(t)\left(\dot{q}_d(t) - \dot{q}(t)\right) \\ + K_d(t)\left(q_d(t) - q(t)\right) = f(t) \end{aligned} \tag{16}$$

where $M_d(t)$, $B_d(t)$, and $K_d(t)$ are the desired inertia, damping, and stiffness matrices, $q_d(t)$ is the desired trajectory, $q(t)$ is the actual trajectory and $f(t)$ is the interaction force and can be measured by the SFS. The acceleration of each joint can be solved by Eq. (15), which can be shown as follows.

$$\ddot{q} = (M(q))^{-1}\left(-C(q,\dot{q})\dot{q} - G(q) + \tau_u + \tau_h\right) \tag{17}$$

Substituting the Eq. (17) into the Eq. (16) so that the control law can be obtained as follows,

$$\begin{aligned} \tau_u(t) = {} & M_d(t)\ddot{q}_d(t) + B_d(t)\left(\dot{q}_d(t) - \dot{q}(t)\right) \\ & + K_d(t)\left(q_d(t) - q(t)\right) - f(t) + C(q(t),\dot{q}(t))\dot{q}(t) \\ & + G(q(t)) - J^T(q(t),\dot{q}(t))f(t) \end{aligned} \tag{18}$$

where $J^T(q(t),\dot{q}(t))$ is Jacobian matrix between interaction force and joint torque.

To develop adaptive learning, a cost function of interaction force and joint error is defined as follows,

$$\Gamma(t) = \left\| e_q(t) - \int_0^t e_f(s)ds \right\|_2 \tag{19}$$

where $e_q(t) = q_d(t)$-$q(t)$ is the angle error and $e_f(t) = f_d(t)$-$f(t)$ is the interaction force error. Due to arbitrary selection of M_d(t) may cause system instability. Therefore, the M_d(t) is fixed to the inertia of the system, and $B_d(t)$ and $K_d(t)$ are updated through the adaptive learning. A gradient descent method is adopted to gradually decrease $\Gamma(t)$ by updating $B_d(t)$ and $K_d(t)$ [32], which can be expressed as follows,

$$\begin{aligned} B_d^k(t) &= B_d^{k-1}(t) - \beta_B \left(\frac{\partial \Gamma^k(t)}{\partial B_d^k(t)}\right)^T \\ &= B_d^{k-1}(t) - \beta_B \left(\frac{\partial f^k(t)}{\partial B_d^k(t)}\right)^T \left(\frac{\partial \Gamma^k(t)}{\partial f^k(t)}\right)^T \\ &= B_d^{k-1}(t) - \beta_B e_q^k(t)\left(\frac{\partial \Gamma^k(t)}{\partial f^k(t)}\right)^T \\ K_d^k(t) &= K_d^{k-1}(t) - \beta_K \left(\frac{\partial \Gamma^k(t)}{\partial K_d^k(t)}\right)^T \left(\frac{\partial \Gamma^k(t)}{\partial f^k(t)}\right)^T \\ &= K_d^{k-1}(t) - \beta_K e_q^{kT}(t)\left(\frac{\partial \Gamma^k(t)}{\partial f^k(t)}\right)^T \end{aligned} \tag{20}$$

where β_B is learning rate of damping parameter update, β_K is learning rate of stiffness parameter update and k is number

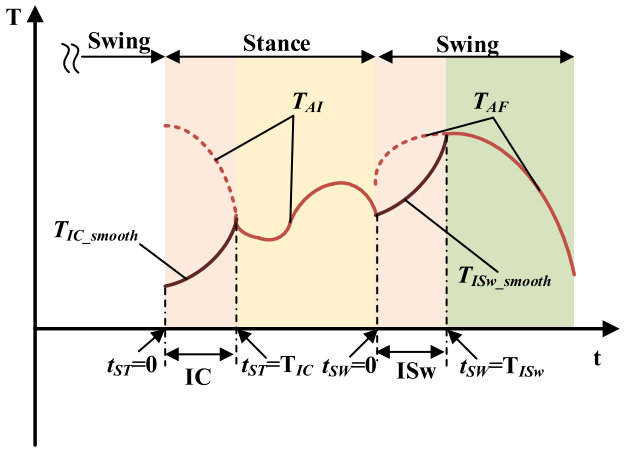

FIGURE 16. Concept of torque smoothing method.

of iterations. According to (19), the gradient of reinforcement can be obtained as follows,

$$\frac{\partial \Gamma^k(t)}{\partial f^k(t)} = \alpha \left(\dot{e}_q(t) - \int_0^t \dot{e}_f(s)ds \right)^T \tag{21}$$

where α is constant. Substituting the Eq. (21) into the Eq. (20) the learning law can be expressed as follows,

$$\begin{aligned} B_d^k(t) &= B_d^{k-1}(t) - \alpha\beta_B \dot{e}_q^{kT}(t) \left(\dot{e}_q(t) - \int_0^t \dot{e}_f(s)ds \right)^T \\ K_d^k(t) &= K_d^{k-1}(t) - \alpha\beta_K e_q^{kT}(t) \left(\dot{e}_q(t) - \int_0^t \dot{e}_f(s)ds \right)^T \end{aligned} \tag{22}$$

B. SMOOTHING METHOD

During human walking, he alternates left and right feet, and the gait phases also cyclically switch. AIC method and ADRC-FTSMC method are used for the stance phase and the swing phase, and there is a sudden change in torque during the two-phase switching process. Therefore when switching between the stance phase and the swing phase, there will be discontinuous torque, which will cause great impact to the wearer. Thus, a smoothing method for modifying the torque is proposed in the IC phase and the ISw phase.

Fig. 16 shows the concept of the torque smoothing method. The control law of the HEXO under the stance phase and swing phases can be implemented by a weighting function as follows,

$$\begin{aligned} T_{ST} &= \begin{cases} T_{AF} + c_{IC\_w}(T_{AI} - T_{AF}) & t_{ST} \le T_{IC} \\ T_{AI} & t_{ST} > T_{IC} \end{cases} \\ T_{SW} &= \begin{cases} T_{AI} + c_{ISw\_w}(T_{AF} - T_{AI}) & t_{SW} \le T_{ISw} \\ T_{AF} + c_{ISw\_}(T_{AF} - T_{AI}) & t_{SW} > T_{ISw} \end{cases} \end{aligned} \tag{23}$$

where t_{SW} and t_{ST} are the elapsed time since the gait phase was detected as the swing phase and the stance phase; T_{IC} and T_{ISw} are the total time to apply the weighting function, which corresponds to the time of the IC phase and the ISW phase; T_{AF} and T_{AI} are the joint torque obtained according to the ADRC-FTSMC method and AIC method; c_{IC_w} and c_{ISw_w} are weight coefficient in IC phase and ISw phase, which can be expressed as follows,

$$\begin{aligned} c_{IC\_w} &= \frac{e^{\alpha_{IC} t_{ST}/T_{IC}} - 1}{e^{\alpha_{IC}} - 1} \\ c_{ISw\_w} &= \frac{e^{\alpha_{ISw} t_{SW}/T_{ISw}} - 1}{e^{\alpha_{ISw}} - 1} \end{aligned} \tag{24}$$

where α_{IC} and α_{ISw} are sensitive factors, which represents the rate of the phase switching.

V. EXPERIMENTS AND DISSCUSSIONS

In order to verify the practical effect and power-assisted ability of the HEXO, three sets of experiments were set up, which include squatting, walking and going up and down stairs. Those are the most common actions in people's daily lives. All experiments were performed under laboratory conditions. The joints angle information, backpack interaction force and plantar interaction force are recorded. The error between the measured joint angle and its desired value is used to evaluate the follow performance of HEXO. Considering that the SFS on the wearable shoes is affected by the ground reaction force in the stance phase, the SFS on the backpack is used to evaluate the support performance of HEXO. Besides, the performance of the HEXO in the anthropomorphic state and the non-personal state is also evaluated.

The wearer and the HEXO are tied by the shoulder straps, belt and wearable shoes. The length of the thigh segment and shank segment are adjusted to ensure the wearer's hip and ankle joints are aligned with the corresponding axis of rotation of the HEXO. The experiments were conducted on four healthy adult volunteers (male, age 26 $\pm$ 3 years old, weight 75 $\pm$ 5 kg, and height 1.75 $\pm$ 0.05 m). HEXO has security protections in both hardware and software. In particularly, all joints are equipped with mechanical restrictions to limit the movement of the joints. For software, the control system will shut down when the drive current exceeds the set limit. In addition, the emergency stop switch is available in emergency.

A. THE SQUATTING EXPERIMENTS

In squatting experiments, subjects wear HEXO in double-leg stance phase, and do the action of squatting down and standing up as shown in Fig. 17. The two feet are fixed and the movement of two legs is consistent. The AIC control strategy was adopted for the experiment. The four volunteers wear the HEXO and completes more than five consecutive squatting down and standing up.

To evaluate the tracking performance of the HEXO, the desired joint angle and the measured joint angle are used to compare. Fig. 18(a) shows the joint angle information of the six squatting action cycles, and Fig. 18(b) shows the following error information of the hip joint and the knee joint. It could be seen that HEXO follows the human movement

FIGURE 17. The experimental process of squatting down and standing up.

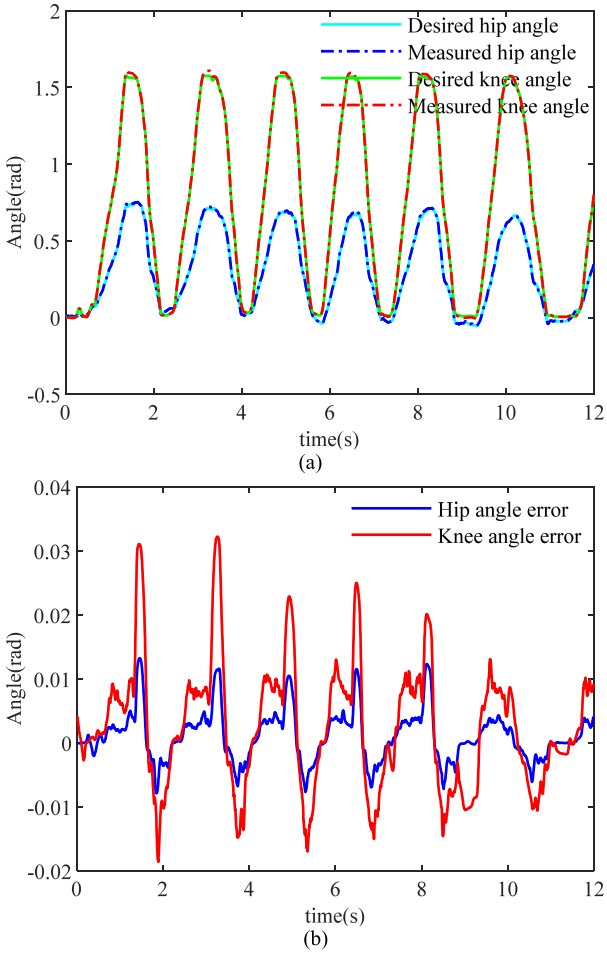

FIGURE 18. Tracking curve of hip and knee angle in the squatting experiments.

smoothly and the tracking errors are converging smaller with the time. In addition, when the HEXO motion is reversed, the joint error is relatively large.

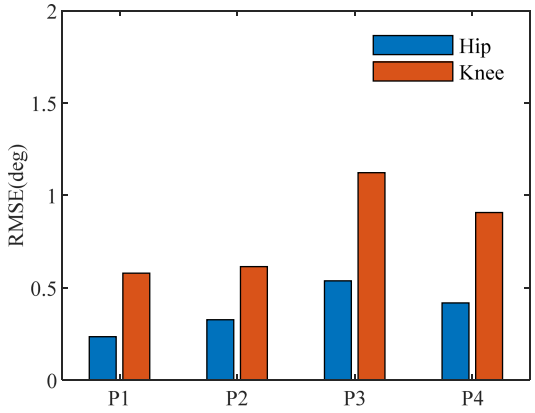

FIGURE 19. The squat tracking performance of four volunteers.

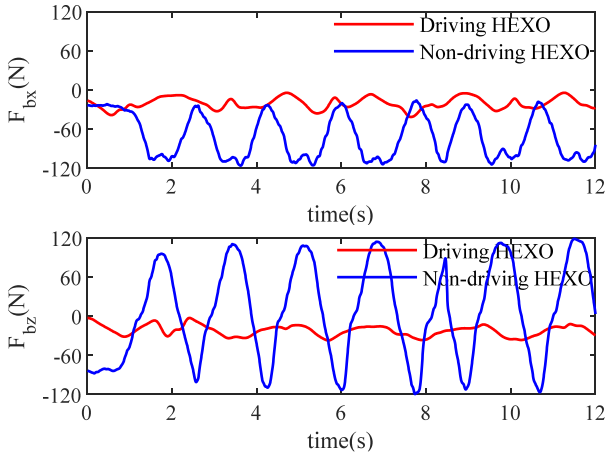

FIGURE 20. The interaction forces of squat experiments in the driving state and the non-driving state.

The root mean square error (RMSE) are used to further evaluate the squatting tracking performance of hip and knee joint, which can be defined as follows,

$$RMSE = \sqrt{\frac{\sum_{k=1}^{N} e(k)^2}{N}} \tag{25}$$

where $e(k)$ is the tracking error and N is the size of error vector. Fig. 19 shows the squatting tracking performance of four volunteers. It could be seen that the hip joint error is smaller than the knee joint error.

To illustrate the support effect of the HEXO, the human-machine interaction force of the backpack is used as the evaluation reference. The force in the vertical direction is F_{bz} and the force in the horizontal direction is F_{bx}. Fig. 20 shows the interaction forces in the driving mode and the non-driving mode. Both modes adopt a non-anthropomorphic structure. Obviously, the interaction force in the driving mode is much smaller than the interaction force in the non-driving mode, which means that the power-assisted effect of HEXO is good. In addition, in order to investigate whether

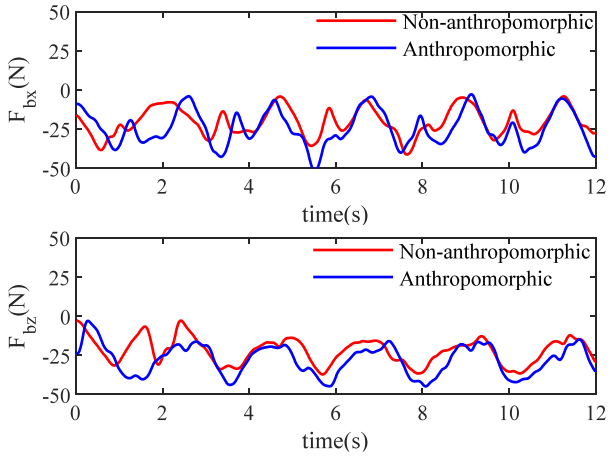

FIGURE 21. The interaction forces of squat experiments in the NAS and AS.

FIGURE 22. The experimental process of walking.

non-anthropomorphic structure is beneficial to improve human machine interaction, we compared the interaction forces in anthropomorphic state (AS) and non-anthropomorphic state (NAS), which is shown in Fig. 21. Both states are in the driving mode. It can be seen that the difference between two states is not obvious.

To quantify the power-assisted effect, the average absolute value (ABV) of interaction forces is used to evaluate, which can be obtained as follows,

$$ABV = \frac{\sum_{i=0}^{n} |F(k)|}{n} \tag{26}$$

where n is number of force sampling points. To further evaluate the performance improvement (P_I), the HEXO in non-driving state as the standard reference and define P_I as follows,

$$P_I = \left(1 - \frac{ABV_1}{ABV_0}\right) \times 100\% \tag{27}$$

where $ABV_0 = [ABV_{0x}\ ABV_{0z}]^T$ is the ABV of horizontal and vertical interaction force in non-driving mode, and $ABV_1 = [ABV_{1x}\ ABV_{1z}]^T$ is the ABV of horizontal and vertical interaction force in driving mode. The statistical results of the four volunteers are shown in Table 4. At the squatting experiments, the two-dimensional forces in driving mode are maintained in a small range of about 30 N. Therefore, the human backpack feels flexible during the squatting process. The mean P_I of F_{bz} in NAS is 64.17%, the mean P_I of F_{bx} in NAS is 62.87%, the mean P_I of F_{bz} in AS is 59.67% and the mean P_I of F_{bx} in AS is 58.86%. It shows the HEXO in NAS can increase the power-assisted effect by 4.5% on the Z-axis and 4.01% on the X-axis compared to the AS.

B. THE WALKING EXPERIMENTS

The squatting experiments have preliminarily verified the feasibility of the AIC control strategy. The ADRC-FTSMC method has been proven in previous work [31]. The continuous walking is more complex as it needs to combine these two methods in a gait cycle. The walking experiments are conducted in the laboratory corridor as shown in Figure 22.

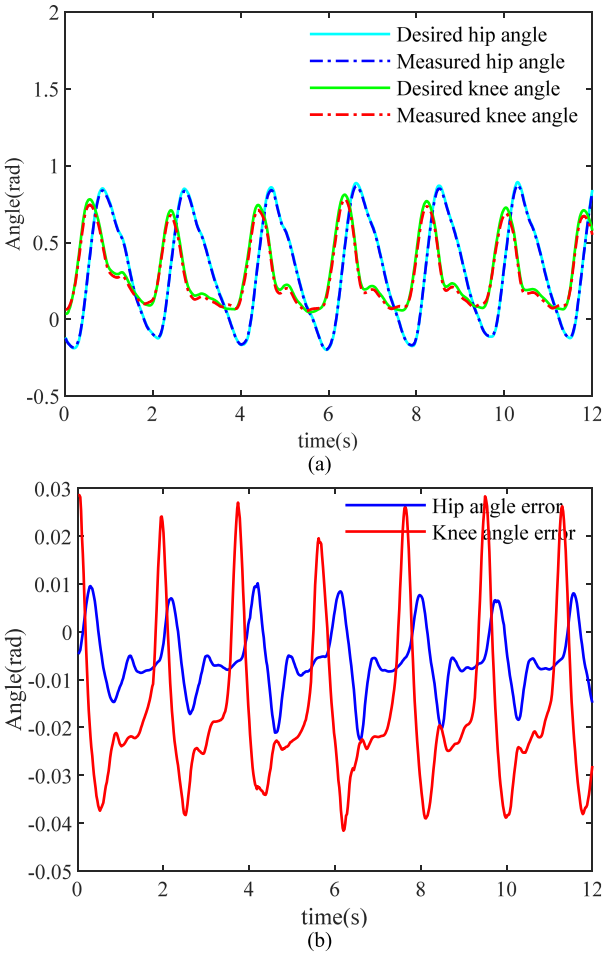

FIGURE 23. Tracking curve of hip and knee angle in the walking experiments.

The curves of the desired angle and the measured angle of the hip and knee joints are shown in Fig. 23 (a). Fig. 23 (b) shows the tracking errors of the hip joint and knee joint

TABLE 4. The statistical results of the squatting experiments.

Sub	*ABV* (N)						P_I			
	Non driving		Driving				P_{I_NAS}		P_{I_AS}	
			NAS		AS					
	Z	X	Z	X	Z	X	Z	X	Z	X
P1	65.34	69.89	22.91	20.62	28.72	24.74	64.94%	70.50%	56.05%	64.60%
P2	68.71	72.38	24.57	23.91	25.52	27.32	64.24%	66.97%	62.86%	62.25%
P3	77.75	74.95	27.54	33.57	29.12	35.33	64.58%	55.21%	62.55%	52.86%
P4	70.45	73.56	26.12	30.29	30.14	32.57	62.92%	58.82%	57.22%	55.72%
Mean	70.56	72.70	25.29	27.10	28.38	29.99	64.17%	62.87%	59.67%	58.86%

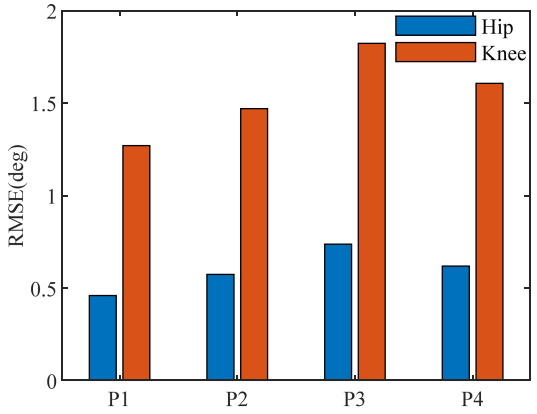

FIGURE 24. The walk tracking performance of four volunteers.

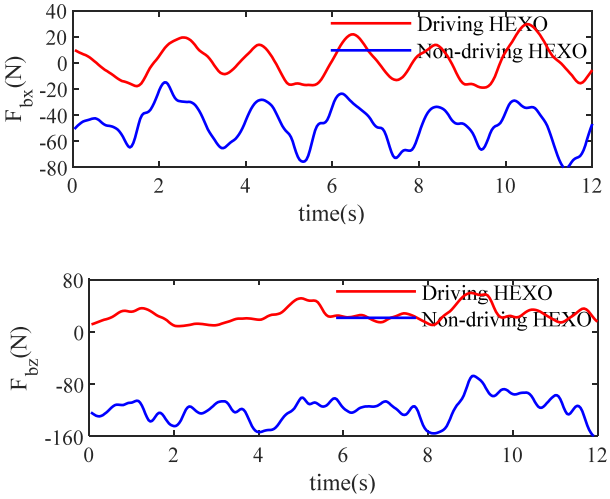

FIGURE 25. The interaction forces of walking experiments in the driving state and the non-driving state.

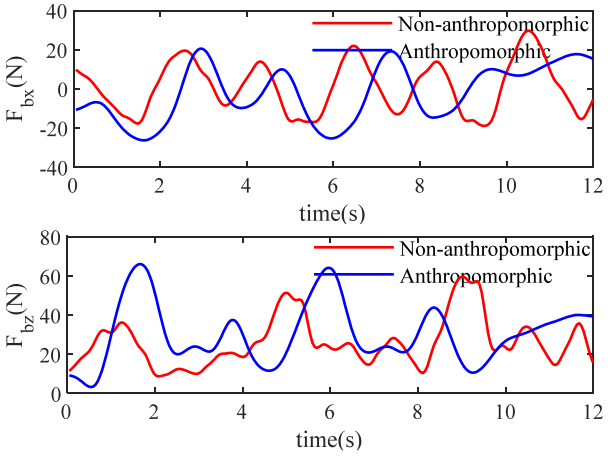

FIGURE 26. The interaction forces of walking experiments in the NAS and AS.

in walking experiments. From this figure, it could be seen that the measured joint angles are nearly consistent with the desired joint angles. The walking curve appears to change periodically and smoothly.

To evaluate the walking tracking performance of hip and knee joint, the RMSE of four volunteers is shown in Fig. 24. The maximum and minimum RMSE of the hip joint are 0.74° and 0.46°, respectively. As for the knee joint, they are 1.82° and 1.27° respectively. These results indicate that the proposed dual-mode control method can control the hip and knee joints to track the walking trajectories well.

Figure 25 shows the interaction forces at the backpack in walking experiments. The blue line shows the interaction force in the non-driving state and the red line indicates the interaction in the driving state. It shows the HEXO in driving state features a good power-assisted effect. High level is the stance phase and low level is the swing phase. The horizontal forces in walking are maintained in a small range of about $\pm$ 20N, which is smaller than the forces in the squatting experiments. This is because the back of the person has small fluctuations in the horizontal direction during walking.

In addition, in order to investigate whether a NAS HEXO in walking experiments is beneficial to improve human machine interaction, the interaction forces in AS and NAS are compared, as shown in Fig. 26.

Furthermore, Table 5 lists the statistical results of the walking experiments. The mean P_I of F_{bz} in NAS is 74.28%, the mean P_I of F_{bx} in NAS is 63.29%, the mean P_I of F_{bz} in AS is 70.21% and the mean P_I of F_{bx} in AS is 54.30%.

During the walking experiments, the human-machine interaction force greatly reduces in the driving state with respect to the non-driving state. The interaction forces in the vertical direction decreases more than the decrease in the horizontal direction, which indicates that the gravity support effect is better. Besides, it shows that the HEXO in NAS can increase the power-assisted effect by 4.06% on the Z-axis and 7.99% on the X-axis compared to the AS. This indicates

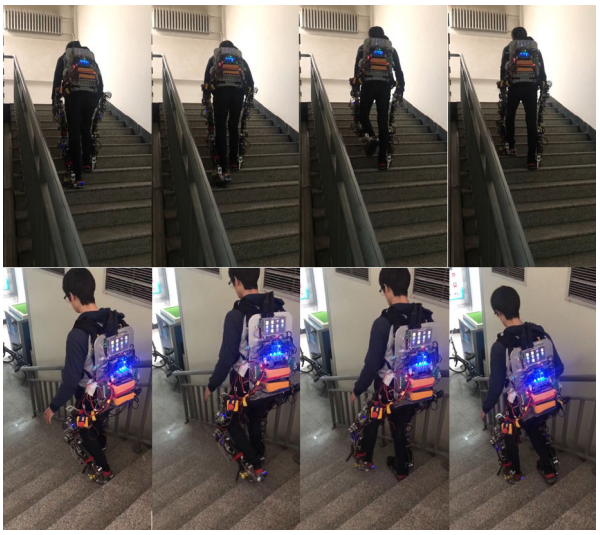

FIGURE 27. The experimental process of up and down stairs.

that HEXO in NAS has a certain improvement on human-machine interaction, which can improve wearing comfort of the HEXO.

C. THE UP AND DOWN STAIRS EXPERIMENT

To further illustrate the universality of the control system, the experiment of up and down stairs is carried out, which is shown in Fig. 27. The control strategy for the up and down stairs is similar to the walking experiments, that is, switching between the swing phase and the stance phase to achieve the function of the up and down stairs.

To ensure the safety of the experiment, the experimental environment was set up as a staircase with handrails. The effect of this control strategy is analyzed by tracking the trajectory, which is generated by the HMI. In addition, in order to analyze the assist effect of the up and down stairs, the interaction of the exoskeleton backs in the driven and undriven states is compared.

Fig. 28 (a) shows the desired trajectory and measured trajectory of the hip and knee joints in the up and down stairs experiments. Fig. 28 (b) shows the following error of the hip joint and the knee joint. To evaluate the tracking performance of hip and knee joints during the up and down stairs experiment, the RMSE of four volunteers is calculated as shown in Fig. 29. The results show that the hip joint RMSE is range from 0.86° to 1.24°, and the knee joint RMSE is range from 1.64° to 2.13°. This shows that the control strategy can also be performed well in the process of going up and down the stairs.

Similarly, in order to analyze the efficiency of the exoskeleton in the up and down stairs, the interaction forces in the non-driving state and driving state are compared. Fig. 30 shows the HEXO in driving state shows a good power-assisted effect. The average vertical interaction force of the HEXO in the driving state is about 20N, which is about 20% of the interaction force in the non-driven state. This means that the

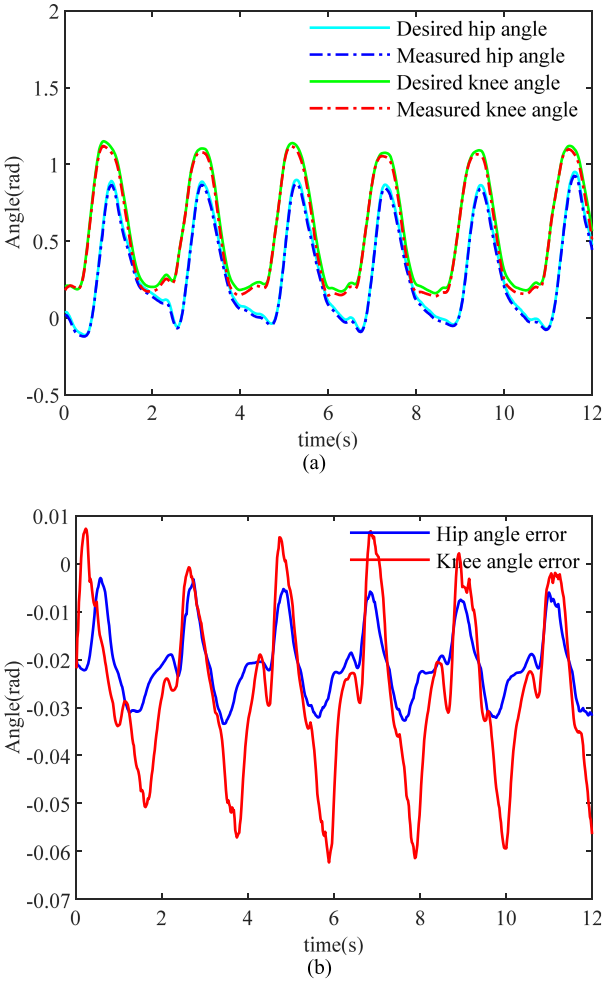

FIGURE 28. Tracking curve of hip and knee angle in the up and down stairs experiments.

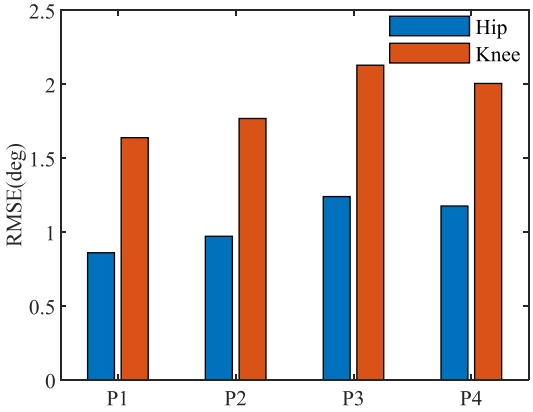

FIGURE 29. The up and down stairs tracking performance of four volunteers.

human body bears a small part of HEXO weight in the driving state.

In order to study the performance of NAS HEXO in the up and down stairs experiment, the interaction forces in AS and NAS are compared, as shown in Fig. 31. Table 6 lists

TABLE 5. The statistical results of the walking experiments.

Sub	*ABV* (N)						P_I			
	Non driving		Driving				P_{I_NAS}		P_{I_AS}	
			NAS		AS					
	Z	X	Z	X	Z	X	Z	X	Z	X
P1	118.48	47.01	26.12	11.10	30.36	12.51	77.95%	76.39%	74.38%	73.39%
P2	117.87	39.92	29.45	15.87	33.41	19.87	75.01%	60.25%	71.66%	50.23%
P3	125.45	50.13	35.81	22.14	42.14	26.57	71.45%	55.83%	66.41%	47.01%
P4	123.76	49.33	33.79	19.40	39.12	24.38	72.70%	60.67%	68.39%	50.58%
Mean	121.39	46.60	31.29	17.13	36.26	20.83	74.28%	63.29%	70.21%	55.30%

TABLE 6. The statistical results of the up and down stairs experiments.

Sub	*ABV* (N)						P_I			
	Non driving		Driving				P_{I_NAS}		P_{I_AS}	
			NAS		AS					
	Z	X	Z	X	Z	X	Z	X	Z	X
P1	129.61	43.65	26.04	15.17	30.62	13.76	79.91%	65.24%	76.38%	68.48%
P2	126.35	41.92	29.17	15.39	32.55	17.06	76.91%	63.29%	74.24%	59.30%
P3	134.72	47.64	34.28	20.22	38.87	23.29	74.55%	57.56%	71.15%	51.11%
P4	132.29	45.01	32.15	18.46	36.76	21.24	75.69%	58.99%	72.21%	52.81%
Mean	130.74	44.55	30.41	17.31	34.70	18.84	76.77%	61.27%	73.49%	57.93%

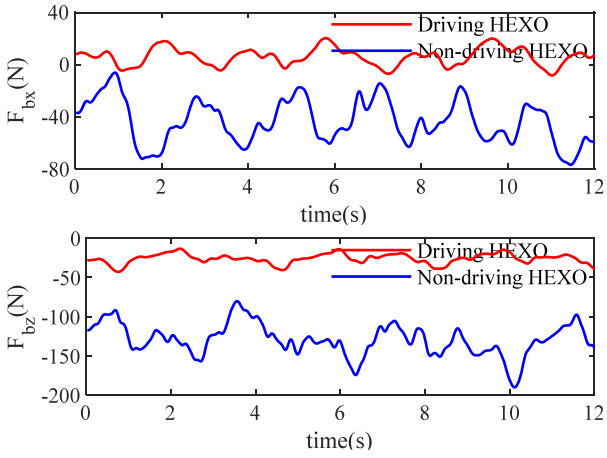

FIGURE 30. The interaction forces of up and down stairs experiments in the driving state and the non-driving state.

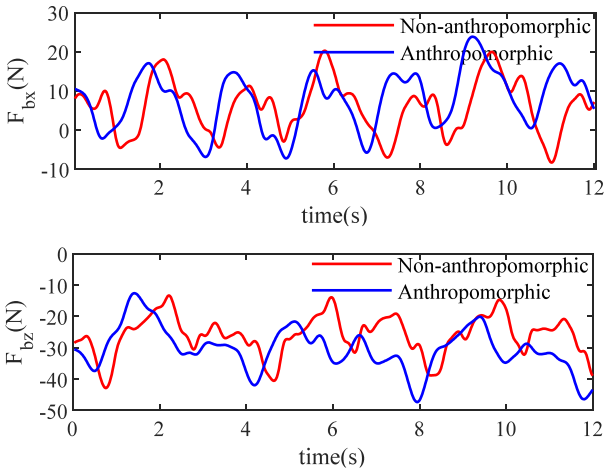

FIGURE 31. The interaction forces of up and down stairs experiments in the NAS and AS.

the statistical results of the up and down stairs experiments. The mean P_I of F_{bz} in NAS is 76.77%, the mean P_I of F_{bx} in NAS is 61.27%, the mean P_I of F_{bz} in AS is 73.49% and the mean P_I of F_{bx} in AS is 57.93%. This shows that the power-assisted effect is obvious during the up and down stairs. Besides, it showed that the HEXO in NAS can increase the assist effect by 3.28% on the Z-axis and 3.34% on the X-axis compared to the AS. This shows that HEXO in NAS can reduce human-machine interaction and improve wearing comfort.

D. DISCUSSION

In order to comprehensively evaluate the performance of the HEXO, we put the results of the three experiments together for analysis. Fig. 32 shows the mean RMSE of four volunteers in three experiments. It could be seen that the mean RMSE of the hip and knee joints were within 2° in three experiments. This shows that the proposed dual-mode control strategy is available in all three experiments. Besides, the mean RMSE of the up and down stairs is the largest, and the mean RMSE of squatting is the smallest, which means that the more complicated the movement is, the greater the tracking error is. In addition, the tracking performance of the knee joint is not as good as that of the hip joint, which may be due to the greater range of motion of the knee joint with respect to the hip joint.

Fig. 33 illustrates the performance improvement of NAS HEXO and AS HEXO in three experiments. It can be clearly seen that HEXO can have better power-assisted effect under the driving state. Especially in the Z-axis direction, the power-assisted effect can reach almost 70%, which means the HEXO can help human body to bear 70% of the load. The best

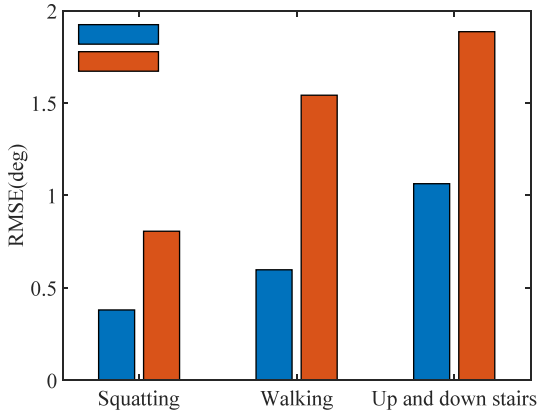

FIGURE 32. The mean RMSE of four volunteers in three experiments.

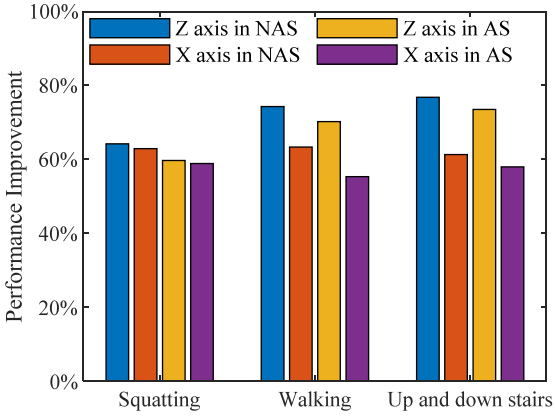

FIGURE 33. The performance improvement of NAS HEXO and AS HEXO in three experiments.

power-assisted effect is the experiments of the up and down stairs, which is also the most needed to provide load support. This shows that the more serious the actual load situation is, the better the power-assisted effect is. In addition, the HEXO in NAS can increase the power-assisted effect by almost 5% compared to the AS. Although it has not greatly improved the overall power-assisted effect, there is still some improvement within a certain range.

VI. CONCLUSION AND FUTURE WORK

In this article, an LLE called HEXO is developed, which is including the overall system design, HMI estimation, and hybrid control. The system design includes mechanical structure design and sensor system design. According to the initial state of the joint angle, HEXO is divided into NAS and AS. The HMI estimation can be divided into gait phase classification and reference trajectory estimation. The hybrid control consists of the AIC in the stance phase and the FTSMC-ADRC in the swing phase. In order to improve the torque discontinuity at the moment of the swing phase and the support phase switching, a smoothing method for modifying the torque is proposed in the IC phase and the ISw phase. In addition, in order to verify the performance of HEXO and the feasibility of the proposed control strategy, three experiments were performed, including squatting, walking and going up and down stairs. The experimental results show that HEXO has a good tracking performance and power-assisted effect by using a hybrid control strategy. Furthermore, the human-machine interaction force of the HEXO in the NAS is smaller than that in the AS. In conclusion, the HEXO can achieve good tracking performance and power-assisted effect according to HMI and hybrid dual-mode control. In addition, the HEXO in the NAS can increase the power-assisted effect to some extent.

In the future, we will choose different control algorithms to experiment on HEXO to compare their respective advantages and disadvantages. Since the experiments are carried out using the same initial angle in NAS, we need to analyze the influence of different initial angles on the system in the future. Since the performance evaluation of HEXO in this paper is mainly based on the tracking effect and the power-assisted effect, we will analyze it from the perspective of human body oxygen consumption and HEXO power consumption in the future.

REFERENCES

[1] T. Yan, M. Cempini, C. M. Oddo, and N. Vitiello, "Review of assistive strategies in powered lower-limb orthoses and exoskeletons," *Robot. Auto. Syst.*, vol. 64, pp. 120–136, Feb. 2015.

[2] Y. Long, Z.-J. Du, C.-F. Chen, W.-D. Wang, and W. Dong, "Development of a lower extremity wearable exoskeleton with double compact elastic module: Preliminary experiments," *Mech. Sci.*, vol. 8, no. 2, pp. 249–258, 2017.

[3] Y. Long, Z.-J. Du, W. Wang, and W. Dong, "Development of a wearable exoskeleton rehabilitation system based on hybrid control mode," *Int. J. Adv. Robot. Syst.*, vol. 13, no. 5, pp. 1–10, 2016.

[4] A. Zoss, H. Kazerooni, and A. Chu, "On the mechanical design of the Berkeley lower extremity exoskeleton (BLEEX)," in *Proc. IEEE/RSJ Int. Conf. Intell. Robots Syst.*, Aug. 2005, pp. 3465–3472.

[5] H. Kazerooni, R. Steger, and L. Huang, "Hybrid control of the Berkeley lower extremity exoskeleton (BLEEX)," *Int. J. Robot. Res.*, vol. 25, nos. 5–6, pp. 561–573, May/Jun. 2006.

[6] Y. Miao, F. Gao, and D. Pan, "Mechanical design of a hybrid leg exoskeleton to augment load-carrying for walking," *Int. J. Adv. Robot. Syst.*, vol. 10, no. 11, p. 395, 2013.

[7] S. C. Jacobsen and M. X. Olivier, "Contact displacement actuator system," WO Patent 2 008 094 191 A2, Aug. 7, 2008.

[8] S. C. Jacobsen, "On the development of XOS, a powerful exoskeletal robot," in *Proc. IEEE/RSJ Int. Conf. Intell. Robots Syst.*, San Diego, CA, USA, 2007, pp. 1441–1469.

[9] H. Kawamoto and Y. Sankai, "Power assist system HAL-3 for gait disorder person," in *Proc. Int. Conf. Comput. Handicapped Persons*, 2002, pp. 196–203.

[10] A. Tsukahara, R. Kawanishi, Y. Hasegawa, and Y. Sankai, "Sit-to-stand and stand-to-sit transfer support for complete paraplegic patients with robot suit HAL," *J. Adv. Robot.*, vol. 24, no. 11, pp. 1615–1638, 2010.

[11] Y. Sankai, "HAL: Hybrid assistive limb based on cybernics," in *Robotics Research* (Springer Tracts in Advanced Robotics). Berlin, Germany: Springer, 2010, pp. 25–34.

[12] Paris, France. *RB3D*. Accessed: Jun. 2015. [Online]. Available: https://www.rb3d.com/wp-content/uploads/2015/06/RB3D_BrochureEXO_HV3_EN_L.pdf

[13] A. Goffer. *Rewalk, More Than Walking*. Accessed: May 2014. [Online]. Available: http://www.rewalk.com/

[14] F. Sergi, D. Accoto, N. L. Tagliamonte, G. Carpino, and E. Guglielmelli, "A systematic graph-based method for the kinematic synthesis of non-anthropomorphic wearable robots for the lower limbs," *Frontiers Mech. Eng.*, vol. 6, no. 1, pp. 61–70, 2011.

[15] A. J. Veale and S. Q. Xie, "Towards compliant and wearable robotic orthoses: A review of current and emerging actuator technologies," *Med. Eng. Phys.*, vol. 38, no. 4, pp. 317–325, 2016.
[16] M. R. Tucker, J. Olivier, A. Pagel, H. Bleuler, M. Bouri, and O. Lambercy, "Control strategies for active lower extremity prosthetics and orthotics: A review," *J. NeuroEng. Rehabil.*, vol. 12, no. 1, p. 1, Jan. 2015.
[17] Z. Li, B. Wang, F. Sun, C. Yang, Q. Xie, and W. Zhang, "SEMG-based joint force control for an upper-limb power-assist exoskeleton robot," *IEEE J. Biomed. Health Inform.*, vol. 18, no. 3, pp. 1043–1050, May 2014.
[18] A. J. Young, L. H. Smith, E. J. Rouse, and L. J. Hargrove, "Classification of simultaneous movements using surface EMG pattern recognition," *IEEE Trans. Biomed. Eng.*, vol. 60, no. 5, pp. 1250–1258, May 2013.
[19] J. Gancet *et al.*, "MINDWALKER: Going one step further with assistive lower limbs exoskeleton for SCI condition subjects," in *Proc. IEEE 4th IEEE RAS EMBS Int. Conf. Biomed. Robot. Biomechatronics*, vol. 49, Jun. 2012, pp. 1794–1800.
[20] J. F. Veneman, R. Kruidhof, E. E. G. Hekman, R. Ekkelenkamp, E. H. F. van Asseldonk, and H. van der Kooij, "Design and evaluation of the LOPES exoskeleton robot for interactive gait rehabilitation," *IEEE Trans. Neural Syst. Rehabil. Eng.*, vol. 15, no. 3, pp. 379–386, Sep. 2004.
[21] A. De Santis, B. Siciliano, A. De Luca, and A. Bicchi, "An atlas of physical human–robot interaction," *Mech. Mach. Theory*, vol. 43, no. 3, pp. 253–270, Mar. 2008.
[22] K. Anam and A. A. Al-Jumaily, "Active exoskeleton control systems: State of the art," *Procedia Eng.*, vol. 41, pp. 988–994, Jul. 2012.
[23] H. Kazerooni, J.-L. Racine, L. Huang, and R. Steger, "On the control of the Berkeley lower extremity exoskeleton (BLEEX)," in *Proc. IEEE Int. Conf. Robot. Automat.*, Apr. 2005, pp. 4353–4360.
[24] L. Wang, S. Wang, E. H. van Asseldonk, and H. van der Kooij, "Actively controlled lateral gait assistance in a lower limb exoskeleton," in *Proc. IEEE/RSJ Int. Conf. Intell. Robots Syst.*, Nov. 2013, pp. 965–970.
[25] L. Wang, Z. Du, W. Dong, Y. Shen and G. Zhao, "Probabilistic sensitivity amplification control for lower extremity exoskeleton," *Appl. Sci.*, vol. 8, no. 4, p. 525, 2018.
[26] Y. Long, Z. Du, C. Chen, W. Wang, L. He, X. Mao, G. Xu, G. Zhao, and X. Li "Development and analysis of an electrically actuated lower extremity assistive exoskeleton," *J. Bionic Eng.*, vol. 14, no. 2, pp. 272–283, Jun. 2017.
[27] Y. Lin, M.-J. J. Wang, and E. M. Wang, "The comparisons of anthropometric characteristics among four peoples in East Asia," *Appl. Ergonom.*, vol. 35, no. 2, pp. 173–178, 2004.
[28] J. Perry and J. R. Davids, "Gait analysis: Normal and pathological function," *J. Pediatric Orthopaedics*, vol. 12, no. 6, p. 815, 1992.
[29] C. Senanayake and S. A. Senanayake, "A computational method for reliable gait event detection and abnormality detection for feedback in rehabilitation," *Comput. Methods Biomech. Biomed. Eng.*, vol. 14, no. 10, pp. 863–874, 2011.
[30] T. Nef, M. Mihelj, G. Kiefer, C. Perndl, R. Muller, and R. Riener, "ARMin—Exoskeleton for arm therapy in stroke patients," in *Proc. IEEE 10th Int. Conf. Rehabil. Robot.*, Jun. 2007, pp. 68–74.
[31] C.-F. Chen, Z.-J. Du, L. He, J.-Q. Wang, D.-M. Wu, and W. Dong, "Active disturbance rejection with fast terminal sliding mode control for a lower limb exoskeleton in swing phase," *IEEE Access*, vol. 7, pp. 72343–72357, 2019.
[32] Y. Li and S. S. Ge, "Impedance learning for robots interacting with unknown environments," *IEEE Trans. Control Syst. Technol.*, vol. 22, no. 4, pp. 1422–1432, Jul. 2014.